Journal of Hydroscience and Hydraulic Engineering
Vol. 1, No. 2, November, 1983, pp.67-82.

INTERPARTICLE STRESSES AND CHARACTERISTICS OF DEBRIS FLOW

By

Toichiro Tsubaki, Haruyuki Hashimoto

Dept. of Civil Engineering Hydraulics and Soil Mechanics,
Kyushu University, Fukuoka 812, Japan

and

Tadashi Suetsugi

Public Works Research Institute, Ministry of Construction, Ibaraki, Japan

SYNOPSIS

Particle-to-particle interactions in a solid-liquid shear flow at high concentration are investigated experimentally in detail, in order to obtain information that could guide the formulation of the constitutive equations. Most of the grains in the flow collide at the `upstream´ quadrant on the surface of the relatively lower grains, and then override them until the grains separate at the `downstream´ quadrant.

The interparticle stresses are conveniently divided into collision stress and contact stress. The former is evaluated theoretically by estimating the momentum transfer in many-body collisions, starting from the analysis of binary collisions. On the other hand, the latter is considered to be isotropic pressure expressed by the grain concentration and be related to the excess immersed weight of grains which can not be supported by the collision normal stress.

By using these results, the characteristics of debris flow such as depth, velocity and concentration are analyzed.

INTRODUCTION

Debris flow is a sediment gravity flow which rapidly carries high concentration of clasts (silt, sand, gravel and boulder) and the interstitial water. For such a granular shear flow, the concept of interparticle stress due to particle-to-particle interactions was introduced by Bagnold (1). He carried out experiments in which neutrally buoyant particles were sheared in a coaxial rotating cylinder apparatus, and obtained semi-empirical formulas for the stresses with some physical considerations.

By applying his formulas for the `grain-inertia´ region to debris flow , several studies were made recently (2,10), notably by Takahashi (10). Since the mechanism of debris flow is closely related to the mechanics of interparticle stresses, more quantitative studies on the interparticle interactions should be made to reach a physically consistent conclusion.

In the mechanics of granular materials, there have been some analytical studies on these stresses. For example, Mctigue (7) attempted to analyze the stresses by making use of the dynamics of binary collisions as interactions among grains. Kanatani's study (6) should be noted in that the quantitative continuum equations were developed on the basis of microscopic properties of the constituent particles. However, his model was simplified under the assumption that frequent collisions between particles were replaced by a succession of random and elastic collisions of a single particle against a rigid spherical wall. Daido (3) attempted to improve Bagnold's simple flow model by applying Kanatani's model to the stresses in debris flow . Recently, Savage and Jeffrey (9) expressed the

stress tensor as an integral containing probability distribution functions for the velocities of the particles and for their spatial arrangement.

Although various approaches to evaluation of the stresses have been proposed so far, there is the lack of experimental information on the mechanism of interparticle interactions in the granular shear flow, especially those in solid-liquid flow.

In the present paper, the interparticle stresses in two-dimensional solid-liquid flow at high concentration and high enough shear rate are theoretically evaluated, based on the microscopic observations of interaction mechanism among grains. By using these results, the characteristics of debris flow such as velocity, depth and grain concentration are analyzed.

Table 1 Experimental conditions of Case A

θ_0	q_{w0} (cm^2/sec)	q_i (cm^2/sec)	U_f (cm/sec)	C_T	H_f (cm)	T_c (sec)
5°	203	16	52.8	0.341	10	0.259
7°	201	19	57.1	0.417	11	0.293
9°	206	24	68.4	0.466	14	0.302

EXPERIMENTS ON INTERPARTICLE INTERACTIONS

Experimental Procedure

A series of experiments (Case A) has been made to obtain information on the generation of interparticle stresses in a solid-liquid shear flow with high concentration of large particles. The flume used was 15cm wide, 30cm deep and 7m long with a transparent acrylite wall on one side, and the slope was variable from 0° to 25°. Nearly spherical mesalite particles were used as a bed material whose mean diameter d_m is 1.74cm and density σ is 1.25 g/cm^3.

Prior to the start of tests, the sediment bed with 8cm depth was saturated with seepage water. By supplying water suddenly at the upstream end of the flume, a flow of the mixture of grains and water started in a bore and traveled rapidly downstream. The flowing profile and the propagation velocity of the bore were recorded by two V.T.R. cameras. Close-up view of the moving grains was taken with a 16mm high-speed camera running at a rate of 100 frames/sec, in order to study the mechanism of interparticle contacts.

The experimental conditions of Case A are summarized in Table 1, in which θ_0 is slope angle of bed, q_i and q_{w0} are discharges of seepage water and fresh water supplied respectively, and U_f, H_f and C_T are velocity, height and grain concentration flux of the bore, respectively.

Mechanism of Interparticle Contacts

To describe the direct interactions among grains quantitatively, we introduce contact angle θ_c defined by the angle between the sloping bed and the tangential plane at the contact point of two contiguous particles, as shown in Fig. 1. An example of the contact angles observed

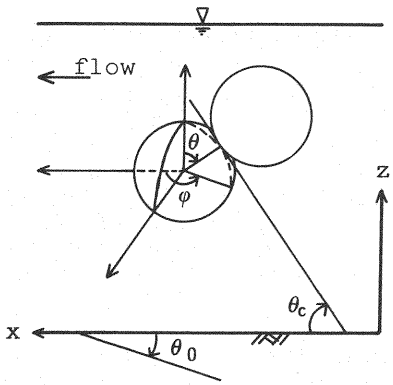

Fig. 1 Definition sketch for contact angle and coordinate system

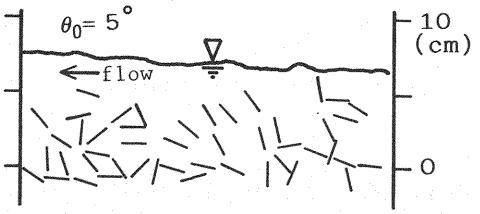

Fig. 2 Example of contact angles

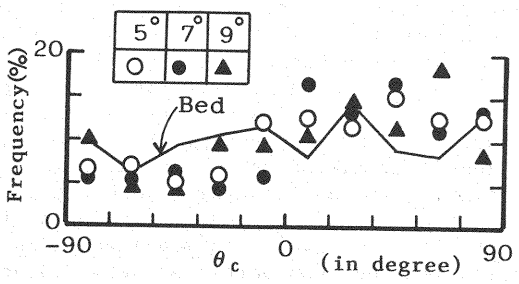

Fig. 3 Frequency distribution of contact angles

in a frame of the film is shown in Fig. 2 by tangential lines at the contact points. The frequency distribution of contact angles obtained from these figures is also shown in Fig. 3, together with that in stationary bed.

Fig. 4 shows some examples of the variation of θ_c obtained every 0.02 sec from the beginning to the end of a grain contact. Herein, the contact angles at the moment of encounter and separation of two grains are expressed as θ_{c*} and θ'_{c*}, respectively. The frequency distributions of θ_{c*} and θ'_{c*} are plotted in Fig. 5. Most of the grains collide at $\theta_{c*} > 0$ with few rebounds and separate at $\theta'_{c*} < 0$, and the frequencies become maximum at $\theta_{c*} \fallingdotseq 45^\circ$ and $\theta'_{c*} \fallingdotseq -45^\circ$, respectively. The mean duration T_c of a contact between two grains is about 0.28 sec as shown in Table 1.

From these measurements, the modes of relative movements after the collisions are classified into five types as follows:

[A] : Two grains keep in contact at constant θ_c for more than 0.1 sec ($\fallingdotseq T_c/3$).

[A']: The duration of constant θ_c is less than 0.1 sec.

[B] : For $\theta_{c*} > 0$, especially $\theta_{c*} = 18^\circ \sim 72^\circ$, the relatively upper grain overrides lower grain with decrease in θ_c.

[C] : For $\theta_{c*} < 0$, the relatively upper grain moves down lower grain with decrease in θ_c.

[D] : If θ_{c*} is near $\pm 90^\circ$, grains alternately move down and up.

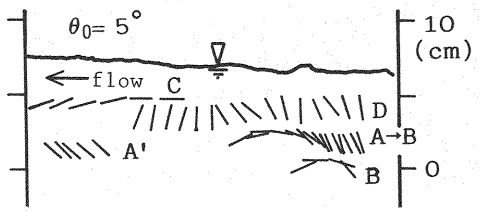

Fig. 4 Variation of contact angles

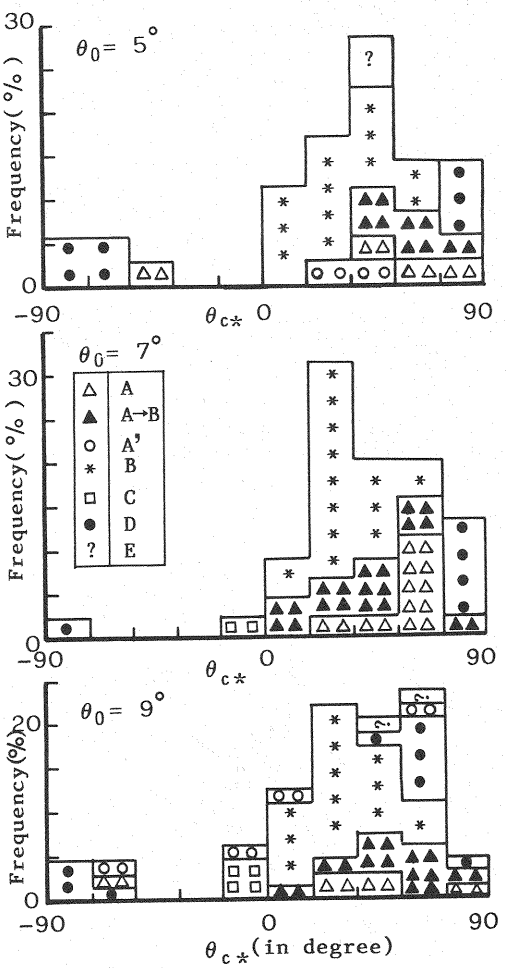

Fig. 6 Frequency distribution of relative movements

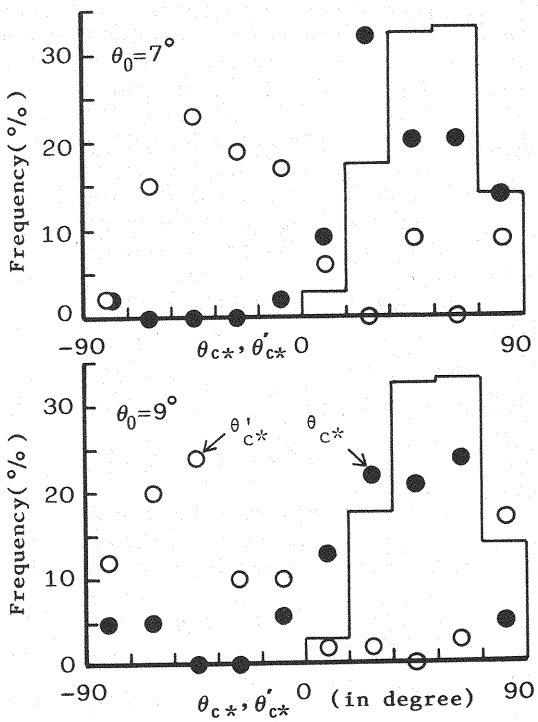

Fig. 5 Frequency distributions of θ_{c*} and θ'_{c*}

Fig. 6 shows the frequency distribution of these modes versus θ_{c*}. Types [A] and [B] are dominant, while the others are negligibly minor. It should be noted that the relative movement of most grains classified in type [A] is converted into type [B] ([A→B]).

Consider a collision for which a reference grain is impacted by a neighbouring grain, as shown in Fig. 7. A spherical coordinate system (r, θ, φ) fixed at the center of the reference grain o is introduced. Using the above results obtained from the close-up view of the contiguous grains near the side wall where they tend to be in contact at $\phi \fallingdotseq 0$ or π, the conclusions are as follows:

1) Grain i being slightly higher in position and having velocity relatively faster than grain o collides on the surface of grain o where $0 < \theta < \pi/2$ and $\pi/2 < \phi < 3\pi/2$. On the other hand, grain i being lower in position collides on the surface where $\pi/2 < \theta < \pi$ and $-\pi/2 < \phi < \pi/2$.

2) For the two-dimensional shear flow, the frequency of collision at constant φ is given by (14)

$$\int_{\theta}^{\theta+\Delta\theta} \sin^2\theta \cos\theta \, d\theta / \int_{0}^{\pi/2} \sin^2\theta \cos\theta \, d\theta = \sin^3(\theta+\Delta\theta) - \sin^3\theta$$

using Eq. 6 described later. The histogram in Fig. 5 is the result calculated with $\Delta\theta = 18^{o}$.

3) Most grains collide at the angle of $\theta_{c*} > 0$, and then override the relatively lower grains until the grains separate at the angle of $\theta'_{c*} < 0$. Therefore, few rebounds at the moment of grain collisions have been observed.

4) According to the observation of the film, the colliding grain i is accompanied by some grains in contact with it. Each accompanying grain also has some grains in contact with it. Therefore, the collision is a many-body one.

ANALYSIS OF INTERPARTICLE STRESSES

From the modes of grain-to-grain interactions mentioned above, the stresses arising from such interactions are conveniently divided into collision stress and contact stress due to the forces acting at the grain collisions and during the subsequent relative movements, respectively. Debris flow is also characterized as a many-body system that grains are linked like a kind of network. Once grain i collides with grain o, as shown in Fig. 7, the momentum must be transmitted to the neighbouring grains through each contact point.

In order to estimate the collisional transport of momentum and to determine the collision stresses, the binary collisions are analyzed at first, and the analysis is extended to the problem of momentum transfer in many-body collisions. On the other hand, as the contacts during the relative movements after grain encounters are not collisional, contact stress is considered to be isotropic stress expressed by the grain concentration in the flow.

Collision Stresses

(a) Collision stresses for two-grain interaction

Consider a collision between grains o and i of equal diameter d as shown in Fig. 7. The change in momemtum of grain i is

$$m(\mathbf{u}'_i - \mathbf{u}_i) = (\mathbf{n} - \mu\mathbf{s}) \int_0^{t_c} F \, dt \qquad (1)$$

in which m is mass of each grain, $\mathbf{u}_i$ and $\mathbf{u}'_i$ are relative velocities of grain i to grain o before and after the collision respectively, **n** and **s** are unit vectors in the direction from the center of grain o to the

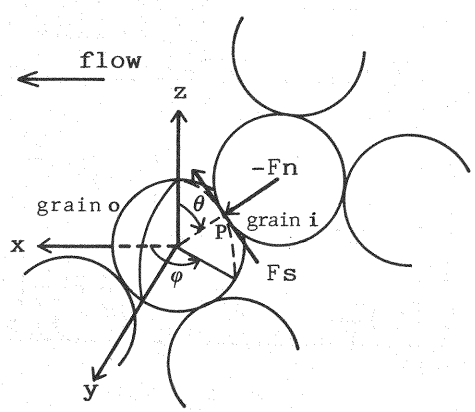

Fig. 7 Definition sketch for collision

collision point P and in the sliding direction of grain i respectively, μ is coefficient of sliding friction, t_c is collision time, and F is normal collision force.

For two-dimensional shear flow u(z), $\mathbf{n}$, $\mathbf{s}$ and $\mathbf{u}_i$ can be written in terms of the spherical coordinates θ and ϕ as

$$\mathbf{n} = (\sin\theta\cos\phi,\ \sin\theta\sin\phi,\ \cos\theta) \tag{2}$$

$$\mathbf{s} = \{\mathbf{u}_i - (\mathbf{u}_i\cdot\mathbf{n})\mathbf{n}\}/\{(\mathbf{u}_i\cdot\mathbf{u}_i) - (\mathbf{u}_i\cdot\mathbf{n})^2\}^{1/2}$$

$$= \{(1-\cos^2\phi\sin^2\theta)^{1/2},\ -\frac{\sin\phi\cos\phi\sin^2\theta}{(1-\cos^2\phi\sin^2\theta)^{1/2}},$$

$$-\frac{\cos\phi\sin\theta\cos\theta}{(1-\cos^2\phi\sin^2\theta)^{1/2}}\}\frac{\cos\theta}{|\cos\theta|} \tag{3}$$

$$\mathbf{u}_i \fallingdotseq (d\cos\theta\,\frac{du}{dz},\ 0,\ 0) \tag{4}$$

By using the no-rebound condition $\mathbf{u}_i'\cdot\mathbf{n} = 0$ at grain collisions and the orthogonal relation $\mathbf{n}\cdot\mathbf{s} = 0$, Eq. 1 reduces to

$$m(\mathbf{u}_i' - \mathbf{u}_i) = -m(\mathbf{u}_i\cdot\mathbf{n})(\mathbf{n} - \mu\mathbf{s}) \tag{5}$$

Grain o receives impulse with the same magnitude as that of grain i but in the opposite direction. The number of collisions of grain o per unit time at the angle within the ranges θ and $\theta+d\theta$, and ϕ and $\phi+d\phi$ is

$$dn = -(d^2\sin\theta\ d\theta\ d\phi\ \mathbf{n}\cdot\mathbf{u}_i)N \tag{6}$$

in which N is number density of grains represented by

$$N = C/(\frac{\pi}{6}d^3) = \beta C/(C_* d^3) \tag{7}$$

in which C and C_* are volumetric concentration of grains in the flow and the stationary bed respectively, and the coefficient β is 1.14 in the present experiments.

With Eqs. 5 and 6, the mean collision force acting on grain o is given by

$$\mathbf{F} = -\int m(\mathbf{u}_i' - \mathbf{u}_i)\,dn$$

$$= -\int_\theta\int_\phi mN(\mathbf{n} - \mu\mathbf{s})(\mathbf{u}_i\cdot\mathbf{n})^2 d^2\sin\theta\ d\theta\ d\phi \tag{8}$$

The interparticle stresses in granular flow are defined as resultant forces acting on either side of the surfaces of grains cut by the plane S of unit area.

Let us consider the collision stress τ_z acting on the plane S_z perpendicular to the z axis. The equation for τ_z is derived as follows:

1) When a grain is cut at the angle θ' by the plane S_z as shown in Fig. 8, the collision force $\mathbf{F}_z(\theta')$ acting on the shaded surface of the grain is described by Eq. 8. The integrations are performed over θ =

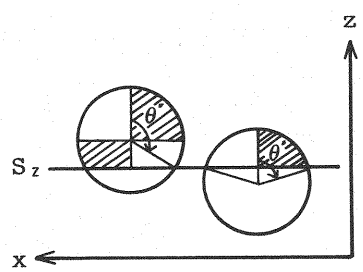

Fig. 8 Definition sketch of θ'

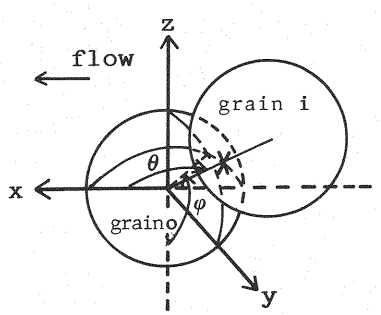

Fig. 9 Redefinition of spherical coordinate

$0 \sim \theta'$ for $\pi/2 < \phi < 3\pi/2$ when $0 < \theta' < /2$, and over $\theta = 0 \sim \pi-\theta'$ for $\pi/2 < \phi < 3\pi/2$ when $\pi/2 < \theta' < \pi$.

2) The number of grains cut by S_z of unit area at the angle within the range θ' and $\theta'+d\theta'$ is given by $N(d/2)\sin\theta' d\theta'$. Thus, τ_z is

$$\tau_z = \int_{\theta'=0}^{\pi} F_z(\theta') N(d/2)\sin\theta' d\theta'$$

$$= -\int_{\phi=\pi/2}^{3\pi/2} d\phi \left(\int_{\theta'=0}^{\pi/2}\int_{\theta=0}^{\theta'} + \int_{\theta'=\pi/2}^{\pi}\int_{\theta=0}^{\pi-\theta'} \right) mN^2 \frac{d^5}{2} \left(\frac{du}{dz}\right)^2 \cdot \mathbf{F}(\theta,\phi) d\theta \sin\theta' d\theta' \qquad (9)$$

in which $\mathbf{F}(\theta,\phi) = (\mathbf{n}-\mu\mathbf{s})\cos^2\theta \sin^3\theta \cos^2\phi$.

The collision stress τ_x acting on the plane S_x perpendicular to the x axis is also given as

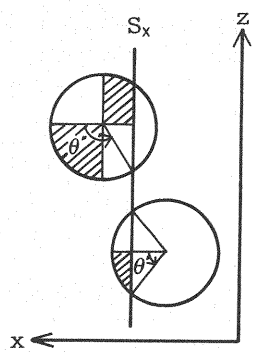

Fig. 10 Definition sketch of θ'

$$\tau_x = -\int_{\phi=-\pi/2}^{\pi/2} d\phi \left(\int_{\theta'=0}^{\pi/2}\int_{\theta=0}^{\theta'} + \int_{\theta'=\pi/2}^{\pi}\int_{\theta=0}^{\pi-\theta'} \right) mN^2 \frac{d^5}{2} \left(\frac{du}{dz}\right)^2 \cdot \mathbf{F}(\theta,\phi) d\theta \sin\theta' d\theta' \qquad (10)$$

in which the spherical coordinate system is redefined as shown in Fig. 9, and the angle θ' is shown in Fig. 10. Therefore, the following equations must be used for $\mathbf{n}$ and $\mathbf{s}$ in $\mathbf{F}(\theta,\phi)$ of Eq. 10.

$$\mathbf{n} = (\cos\theta, \sin\theta\sin\phi, -\sin\theta\cos\phi)$$

$$\mathbf{s} = (-\sin\theta, \cos\theta\sin\phi, -\cos\theta\cos\phi)\frac{\cos\phi}{|\cos\phi|}$$

After some complicated calulations, stress components are described by

$$\tau_{jk} = \beta^2 \frac{m}{d} \left(\frac{C}{C_*}\right)^2 \left(\frac{du}{dz}\right)^2 A_{jk} \qquad (11)$$

$$\begin{vmatrix} A_{xx} & A_{xz} \\ A_{zx} & A_{zz} \end{vmatrix} = \begin{vmatrix} -0.0898-0.089\mu & 0.0762-0.076\mu \\ 0.0762+0.102\mu & -0.0898+0.067\mu \end{vmatrix}$$

(b) Momentum transfer for many-grain interaction

Let us term grain i impacting grain o `1st-order grain´. `2nd-order grain´ is defined to be grains in contact with 1st-order one, `3rd-order grain´ be grains in contact with 2nd-order one, and so on. If the collision between grains o and i happens, then the change in momentum of each grain is

$$\begin{aligned}
m\,d\mathbf{u}_1 &= (\mathbf{n}-\mu\mathbf{s})\,F\,dt + \sum_{1}^{N_2} \mathbf{E}_{2,1}dt \\
m\,d\mathbf{u}_2 &= \mathbf{E}_{1,2}dt + \sum_{2}^{N_3} \mathbf{E}_{3,2}dt \\
&\cdots\cdots\cdots\cdots \\
m\,d\mathbf{u}_l &= \mathbf{E}_{l-1,l}dt + \sum_{1}^{N_{l+1}} \mathbf{E}_{l+1,l}dt \\
m\,d\mathbf{u}_{l+1} &= \mathbf{E}_{l,l+1}dt + \sum_{l+1}^{N_{l+2}} \mathbf{E}_{l+2,l+1}dt
\end{aligned} \qquad (12)$$

in which $d\mathbf{u}_j$ is velocity change of jth-order grain, $\mathbf{E}_{j,j+1}$ is force acting on (j+1)th-order grain from jth-order one, and ${}_jN_{j+1}$ is number of (j+1)th-order grains in contact with jth-order one.

Obviously $\mathbf{E}_{j+1,j} = -\mathbf{E}_{j,j+1}$, and we assume the following relation in Eq. 12.

$$F > \sum_{1}^{N_2} |\mathbf{E}_{2,1}|,\ |\mathbf{E}_{1,2}| > \sum_{2}^{N_3} |\mathbf{E}_{3,2}|,\ \cdots\cdots,\ |\mathbf{E}_{l,l+1}| > \sum_{l+1}^{N_{l+2}} |\mathbf{E}_{l+2,l+1}|$$

Adding each equation in Eq. 12 and considering the above relations yields

$$m(du_1 + \sum_{1N_2} du_2 + \cdots\cdots + \sum_{1N_2}\sum_{2N_3}\cdots\cdots\sum_{1N_{l+1}} du_{l+1})$$
$$= (\mathbf{n} - \mu\mathbf{s})F\,dt + \sum_{1N_2}\sum_{2N_3}\cdots\cdots\sum_{l+1N_{l+2}} E_{l+2,l+1}\,dt$$
$$\fallingdotseq (\mathbf{n} - \mu\mathbf{s})F\,dt \qquad (13)$$

For the process of the momentum transfer, the following relation is assumed.

$$\sum_{1N_2} du_2/du_1 = \sum_{2N_3} du_3/du_2 = \cdots\cdots = \sum_{1N_{l+1}} du_{l+1}/du_1 = \varepsilon$$

in which $0 < \varepsilon < 1$. Eq. 13 thus reduces to

$$m(1 + \varepsilon + \varepsilon^2 + \cdots\cdots + \varepsilon^l)du_1 = (\mathbf{n} - \mu\mathbf{s})\quad F\,dt \qquad (14)$$

As $l \to \infty$, Eq. 14 becomes

$$\frac{m}{1-\varepsilon}(\mathbf{u}_1' - \mathbf{u}_1) = (\mathbf{n} - \mu\mathbf{s})\int_0^{tc} F\,dt \qquad (15)$$

in which $\mathbf{u}_1$ and $\mathbf{u}_1'$ are velocities of grain i before and after the collision with grain o, respectively.

Comparing Eq. 15 with Eq. 1, it is found that the mass of a grain in many-body system must be replaced by $M=m/(1-\varepsilon)$ due to the effects of many-body collisions on momentum transfer. Since ε approaches 1 as $C \to C_*$, ε may be expanded in a Taylor series about $C=C_*$.

$$\varepsilon = 1 + \frac{\partial\varepsilon}{\partial C}(C - C_*) + \cdots\cdots \fallingdotseq 1 + \frac{1}{k_M}\frac{C - C_*}{C_*}$$

in which k_M is a constant determined later. As a first approximation, M is described by

$$M = m\,\frac{k_M}{1 - C/C_*} \qquad (16)$$

Thus, collision stress components are given by Eq. 11, into which M is substituted for m.

Contact Stress

Contact stress due to the grain contacts during the relative movements after the collisions may be determined by both the number of contact points n_c on a single particle and the contact force exerted on it from a neighbouring one. Considering that the geometrical distribution of contact points except those of collisions is nearly uniform (Fig. 3) and neglecting the minor role of contact shear stress, the contact pressure p can be obtained on referring to Eq. 9 and Fig. 8 as follows:

$$p = \int_0^{\pi}\left[\int_0^{\theta'}\frac{n_c F'}{\pi d^2}\cos\theta\,\pi\frac{d^2}{2}\sin\theta\,d\theta\right]\frac{d}{2}N\sin\theta'\,d\theta'$$
$$= \frac{1}{6}n_c d\,F'N$$
$$= (C_* n_c' F')\left(\frac{C}{C_*}\right) \qquad (17)$$

in which $n_c'=n_c/(\pi d^2)$ is density of contact points on a grain and F' is the normal contact force at each contact point. Since the strict estimation of $n_c'F'$ is very difficult, it may be evaluated under the following physical consideration: If the collisions were elastic, the dispersed grains could be supported by only the collision stress. However, because of completely inelastic collisions as aforementioned, $n_c'F'$ may be generated by the excess immersed weight of grains which cannot be supported by the collision normal stress, and related to the grain concentration.

The contact pressure should vanish as $C \to C_s$, where C_s is the grain concen-

tration at the free surface. $C_* n'F'$ can be expanded in power series of C about C= C_s. The following relation is derived as a crude approximation:

$$p = K_p \frac{C}{C_*} \frac{C - C_s}{C_s} \tag{18}$$

in which $K_p C/C_*$ formally corresponds to a bulk modulus in the area of continuum mechanics. For the functional form of K_p, the relation $K_p \propto (\sigma-\rho)\, gh\cos\theta_0$ has been inferred dimensionally from the above considerations, in which ρ is density of fluid and h is flow depth.

Thus the interparticle stress components σ_{jk} are given by

$$\sigma_{jk} = \tau_{jk} - p\,\delta_{jk}$$

$$= \beta^2 \frac{m}{d} k_M \frac{(C/C_*)^2}{1 - C/C_*} \left(\frac{du}{dz}\right)^2 A_{jk} - K_p \frac{C}{C_*} \frac{C - C_s}{C_s} \delta_{jk} \tag{19}$$

in which δ_{jk} is the Kronecker delta.

Comparison With Bagnold's Formula (1)

Bagnold sheared neutrally buoyant spherical particles in a coaxial rotating cylinder apparatus and measured both the torque and the normal stress in the radial direction at the various concentration of particles. In the 'grain-inertia' region which is relevant to the present study, he gave the formulas for the stresses

$$\left.\begin{aligned} \sigma_{zx} &= a \sin\alpha_B\, \sigma\, d^2 \{(\frac{C}{C_*})^{1/3} - 1\}^{-2} (\frac{du}{dz})^2 \\ &= \sigma_{zz} \tan\alpha_B \end{aligned}\right\} \tag{20}$$

in which α_B is dynamic angle of internal friction and a is numerical constant, with the values of $\tan\alpha_B$=0.32 and a=0.042, respectively. On the other hand, the collision shear stress in the present analysis is

$$\sigma_{zx} = (0.0762+0.102\mu) \frac{\pi}{6} \beta^2 k_M \sigma d^2 \cdot \frac{(C/C_*)^2}{1 - C/C_*} \left(\frac{du}{dz}\right)^2 \tag{21}$$

The calculated result of the present theory together with the Bagnold's one is shown in Fig. 11 in the form of nondimensional stress versus C/C_*. Since they agree well for k_M=7.5 and μ=0.1, the value of k_M is inferred as about 7.5 for debris flow.

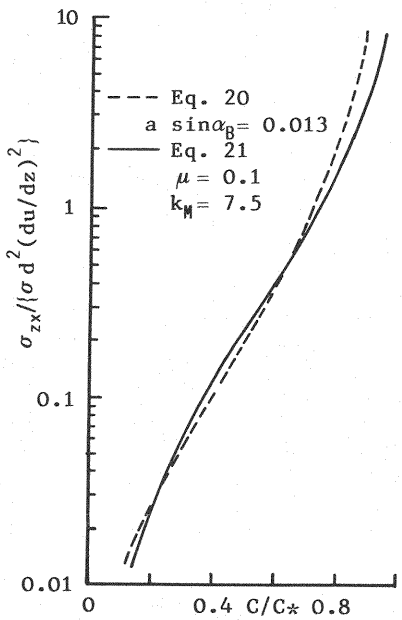

Fig. 11 Comparison of present theory with Bagnold's one

FLOW PROPERTIES OF DEBRIS FLOW

Experiments on the Movement of Debris Flow

(a) Experimental method

In order to investigate the nature of debris flow in detail, two series of experiments with mesalite (Case B) and sand (Case C) as a bed material were conducted. The flume and the experimental procedure were almost same as those of Case A aforementioned. Items of the experiments are summarized in Table 2, where Φ is angle of repose of grains in water, and θ_{0i} and θ_{0*} are critical slope angles for the occurrence of debris flow and for the instability of the whole sediment bed layer, respectively. Both the slope angles are given by Takahashi(10) as

Table 2 Experimental conditions for debris flow

	d_m (mm)	σ (g/cm^3)	C_*	$\tan\Phi$	θ_{0i}	θ_{0*}	q_{w0} (cm^2/sec)	θ_0	U_f (cm/sec)	H_f (cm)
Case B	8.2	1.6	0.59	0.78	5.9°	11.5°	200	4°~12°	70 ~ 90	5 ~ 12
Case C	4.6	2.59	0.58	0.73	11.7°	19.3°	200	12°~23°	100 ~ 150	3 ~ 11

$$\tan\theta_{0i} = \frac{C_*(\sigma - \rho)}{C_*(\sigma - \rho) + \rho(1 + 1/\kappa)} \tan\Phi$$

with $\kappa = 0.75$, and

$$\tan\theta_{0*} = \frac{C_*(\sigma - \rho)}{C_*(\sigma - \rho) + \rho} \tan\Phi$$

The distributions of grain velocity and concentration were measured by filming the flow with the 16mm high- speed camera running at a rate of 100 ~ 200 frames/sec.

Referring to the method by Hirano and Iwamoto (5), the measurements of the grain concentration distribution were made as follows: 1) Only one layer of the grains in contact with the side wall was photographed by supplying white water colored by small amount of white paint; 2) From the photograph of the flow, we divided the whole region into several rectangles of equal area and counted the number of grains N_A in each rectangle; 3) N_A was transformed into concentration with the relation $C=C_*(N_A/A)^{3/2} d^3/\beta$, in which A is the area of a rectangle.

Discharge and concentration flux of the debris flow were measured at the downstream end of the flume by catching the flow in a bucket.

(b) Experimental results

In the following discussion, x is taken in the direction of flow and z is vertically upward from the bottom, as shown in Fig. 1.

The vertical distribution of concentration C/C_b measured in Case B is plotted in Fig. 12, in which $\eta=z/h$ and C_b is concentration at the bottom $\eta=0$. Although there is wide scatter in the experimental values and remains doubts on the accuracy of concentration estimated from particle number in contact with the wall, it should be noted that the concentration gradient in debris flow becomes larger with decrease in the slope angle θ_0.

Examples of the grain velocity profile u/u_s are plotted in Fig. 13 (a), (b) and (c), in which u_s is velocity at the free surface. It is clear that debris flow is characterized by grain velocity profile, which is convex upward in the lower part of the flow and inversely downward in the upper part, and thus has an inflection point. Because of the asymptotic decrease of velocity near the movable bed, it is difficult to decide the position of the bottom. In the present study, z=0 has been conveniently taken at the elevation where the flow velocity is about $0.03u_s$, after some trials.

The broken lines in these figures show the analytical solutions which Takahashi (10) derived. According to the theory, the grain concentration is uniformly distributed with respect to z and is expressed as

$$C = C_T = \frac{\tan\theta_0}{\{(\sigma - \rho)/\rho\}(\tan\Phi - \tan\theta_0)} \qquad (22)$$

in which C_T is concentration flux defined later by Eq. 39. The velocity profile is given by

$$u/u_s = 1 - (1 - \eta)^{3/2} \qquad (23)$$

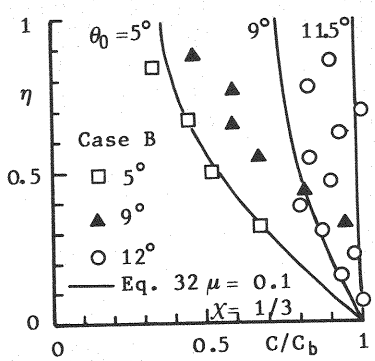

Fig. 12 Distribution of concentration

Analysis on the Distribution of Grain Concentration and Velocity

The basic equations for the two-dimensional steady and uniform flow are written as

$$\{\sigma C + \rho(1 - C)\}g \sin\theta_0 + \frac{\partial \sigma_{zx}}{\partial z} + (1 - C)\frac{\partial \sigma^w_{zx}}{\partial z}$$

$$- \frac{\partial}{\partial z}\{\rho(1 - C)\overline{u'_w w'_w}\} = 0 \qquad (24)$$

$$- (\sigma - \rho)Cg \cos\theta_0 + \frac{\partial \sigma_{zz}}{\partial z} + I_z = 0 \qquad (25)$$

In the above equations, both the viscous stress σ^w_{zx} and Reynolds stress $-\overline{u'_w w'_w}$ in the interstitial fluid are assumed to be negligibly minor. I_z in Eq. 25 is due to an interaction force between grains and fluid. It consists of two main forces caused by relative velocity between grains and fluid and by added mass at the grain collisions. While the former force is neglected because of minor role, the latter is considered by substitution of $m(1+\rho/2\sigma)$ for m in σ_{zz} of Eq. 19. The stresses σ_{zx} and σ_{zz} are expressed as

$$\sigma_{zx} = \tau_{zx} = K_M \sigma d^2 \frac{(C/C_*)^2}{1-C/C_*}\left(\frac{du}{dz}\right)^2 \qquad (26)$$

with $K_M = \frac{\pi}{6}(0.0762+0.102\mu)\beta^2 k_M$, and

$$\left.\begin{aligned} \sigma_{zz} &= \tau_{zz} - p \\ p &= K_p \frac{C}{C_*}\frac{(C - C_s)}{C_s} \end{aligned}\right\} \qquad (27)$$

For convenience, we put

$$\frac{\tau_{zx}}{\tau_{zz}} = -\frac{\gamma}{1 + \rho/(2\sigma)} = -\alpha \qquad (28)$$

in which $\gamma = \frac{0.0762+0.102\mu}{0.0898-0.067\mu}$.

(a) Distribution of grain concentration

Substituting Eqs. 26 ~ 28 into Eqs. 24 and 25, the concentration gradient is given by

$$\frac{K_p}{C_s(\sigma - \rho)gh\cos\theta_0}\frac{dC}{d\eta} = -\frac{\alpha - \tan\theta_0}{\alpha} \cdot C_* \frac{C - C_\alpha}{2C - C_s} \qquad (29)$$

in which C_α denotes the concentration for p=0 (K_p = 0) and is written as

$$C_\alpha = \frac{\tan\theta_0}{\{(\sigma - \rho)/\rho\}(\alpha - \tan\theta_0)} \qquad (30)$$

The boundary condition of debris flow over movable beds is taken to be u=0 and $C=C_*$

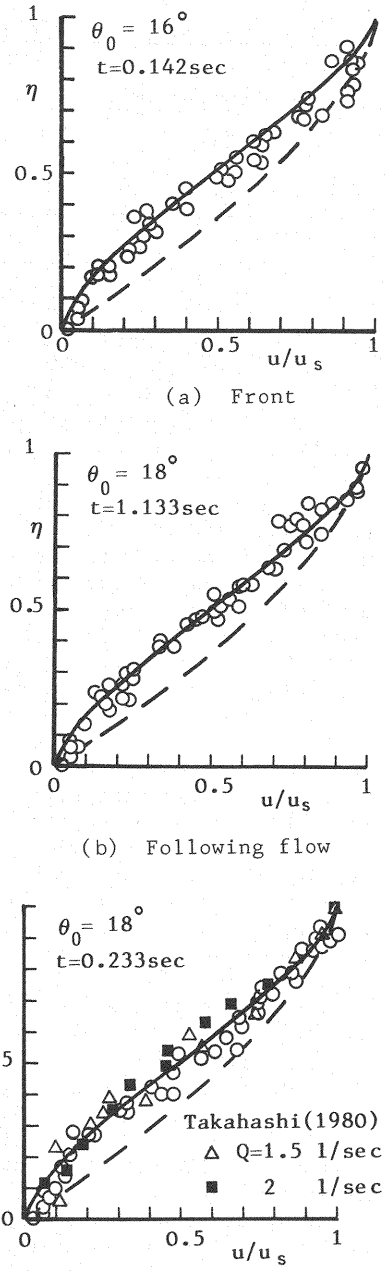

Fig. 13 Velocity profile (Case C); t is elapsed time from passage of the front of debris flow past the measuring station.

at the bottom z=0. Putting

$$\frac{K_p}{C_s(\sigma - \rho)gh\cos\theta_0} = \chi \; ; \qquad \frac{\alpha - \tan\theta_0}{\alpha} = \psi \tag{31}$$

and assuming χ to be a constant, the integration of Eq. 29 yields

$$\eta = \left(2\,\frac{C_* - C}{C_*} - \frac{2C_\alpha - C_s}{C_*}\,\ln\frac{C - C_\alpha}{C_* - C_\alpha}\right)\frac{\chi}{\psi} \tag{32}$$

Putting $C=C_s$ at $\eta=1$ in Eq. 32, the surface concentration is given by

$$\frac{C_s - C_\alpha}{C_* - C_\alpha} = \exp\left\{\left(2\,\frac{C_* - C_s}{C_*} - \frac{\psi}{\chi}\right)C_*/(2C_\alpha - C_s)\right\} \tag{33}$$

Integrating Eq. 32, average concentration $\bar{C}$ becomes

$$\bar{C} = C_\alpha + (C_* - C_s)\,\frac{\chi}{\psi} \tag{34}$$

(b) Velocity profile

Integrating Eq. 24 by use of Eqs. 26 and 29, the following equation is obtained.

$$\frac{d}{d\eta}\left(\frac{u}{u_*}\right) = \frac{h}{d}\left(K_M\,\frac{\sigma}{\rho}\,\frac{\psi}{\chi}\,C_*\right)^{-1/2}\frac{(1 - C/C_*)^{1/2}}{C/C_*}\Big[(C - C_s)\Big\{\frac{\sigma - \rho}{\rho}(C + 2C_\alpha) + 2\Big\}$$

$$+ \left(1 + \frac{\sigma - \rho}{\rho}\,C_\alpha\right)(2C_\alpha - C_s)\,\ln\frac{C - C_\alpha}{C_s - C_\alpha}\Big]^{1/2} \tag{35}$$

in which $u_*=\sqrt{gh\sin\theta_0}$ is shear velocity. It is found that velocity gradient becomes zero at both the free surface and the bottom.

Utilizing Eq. 29, u/u_* can be solved under the boundary condition of $u=0$ at $\eta=0$, i.e. $C=C_*$.

$$\frac{u}{u_*} = \frac{h}{d}\Big\{\frac{\sigma}{\rho}\,K_M\,\left(\frac{\psi}{\chi}\,C_*\right)^3\Big\}^{-1/2}\int_C^{C_*} F(C)\,dC \tag{36}$$

in which

$$F(C) = \frac{2C - C_s}{C - C_\alpha}\,\frac{(1 - C/C_*)^{1/2}}{C/C_*}\Big[(C - C_s)\Big\{\frac{\sigma - \rho}{\rho}(C + 2C_\alpha) + 2\Big\}$$

$$+ \left(1 + \frac{\sigma - \rho}{\rho}\,C_\alpha\right)(2C_\alpha - C_s)\,\ln\frac{C - C_\alpha}{C_s - C_\alpha}\Big]^{1/2}$$

Eq. 36 becomes a function of η by using Eq. 32. Putting $C=C_s$ and $u=u_s$ in Eq. 36, the surface velocity is obtained. The dimensionless velocity profile may be written as

$$\frac{u}{u_s} = \int_C^{C_*} F(C)\,dC \Big/ \int_{C_s}^{C_*} F(C)\,dC \tag{37}$$

Integrating Eq. 36 with respect to η, average velocity $\bar{u}$ becomes

$$\frac{\bar{u}}{u_*} = \frac{h}{d}\Big\{\frac{\sigma}{\rho}\,K_M\,\left(\frac{\psi}{\chi}\,C_*\right)^5\Big\}^{-1/2}\int_{C_s}^{C_*}\frac{2C - C_s}{C - C_\alpha}\Big(\int_C^{C_*} F(C)\,dC\Big)dC \tag{38}$$

(c) Grain concentration flux

Writing fluid velocity as u_w, concentration flux C_T is defined by

$$C_T = \int_0^1 C\,u\,d\eta \Big/ \int_0^1 \{C\,u + (1 - C)u_w\}\,d\eta \tag{39}$$

Considering $u \doteqdot u_w$, Eq. 39 becomes

$$C_T = \int_0^1 C\,u\,d\eta \Big/ \int_0^1 u\,d\eta$$

$$= \int_{C_s}^{C_*} \frac{C(2C - C_s)}{C - C_\alpha} \left(\int_C^{C_*} F(C)\,dC\right)dC \Big/$$

$$\int_{C_s}^{C_*} \frac{2C - C_s}{C - C_\alpha} \left(\int_C^{C_*} F(C)\,dC\right)dC \qquad (40)$$

Fig. 14 shows the experimental results of C_T in Cases B and C. In order to calculate the above equations, we must determine the values of the coefficient μ of sliding friction at collisions and χ defined by Eq. 31. After some trial calculations of Eq. 40, the following two features of μ and χ have been found. First, the gradient between C_T versus $\tan\theta_0$ is determined predominantly by χ. Secondly, bed slope such that $C_T = C_*$ is prescribed by μ.

Noting these features, C_T is calculated versus $\tan\theta_0$ for various values of μ and χ. As a result, good agreement is found between calculated and experimental values if $\mu = 0.1$ and $\chi = 1/3$, as shown in Fig. 14. The theoretical curves of concentration distribution and velocity profile calculated by using these values are shown in Figs. 12 and 13, respectively. Agreements between the theory and the experiments are reasonable.

Characteristics of Debris Flow

According to Takahashi's theory (10), the average velocity is given by

$$\frac{\bar{u}}{u_*} = \frac{2}{5\sqrt{a \cdot \sin\alpha_B}} \frac{h}{d} \left\{ C + (1 - C)\frac{\rho}{\sigma} \right\}^{1/2} \left\{ \left(\frac{C_*}{C}\right)^{1/3} - 1 \right\} \qquad (41)$$

in which $a \cdot \sin\alpha_B$ is assumed to be 0.02 (11). The average velocity by the present analysis is described as Eq. 38. The equations for the moving velocity and the height of the bore are obtained as follows: Replacing $\bar{u}$ and h in Eq.38 by U_f and H_f, dimensionless moving velocity $(U_f/\sqrt{gH_f \sin\theta_0})d/H_f$ becomes a function of C_T (or $\tan\theta_0$) with parameters of σ/ρ, μ, χ and k_M. Figs. 15(a) and (b) show the results of the dimensionless velocity calculated by Eq. 38 with $\mu = 0.1$, $\chi = 1/3$ and $k_M = 5$, together with the experimental results.

The total discharge per unit width at the debris front $q_t = U_f H_f$ is prescribed by the supplied water discharge q_{w0} as

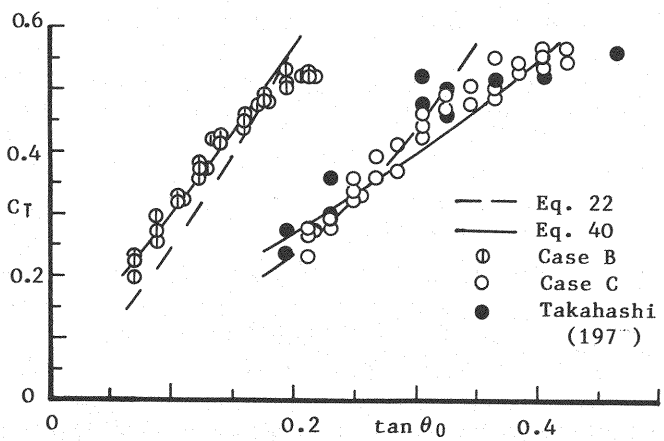

Fig. 14 Concentration flux versus bed slope

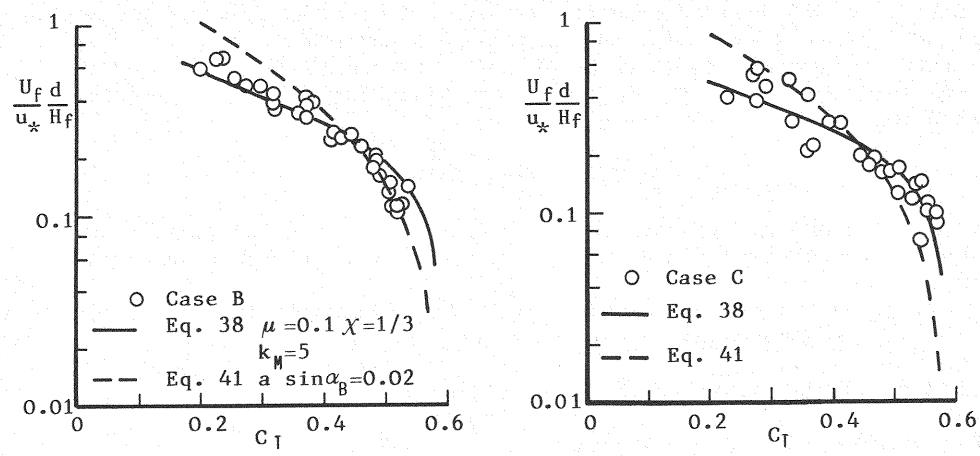

(a) Case B (mesalite) (b) Case C (sand)

Fig. 15 Nondimensional moving velocity of debris bore versus C_T

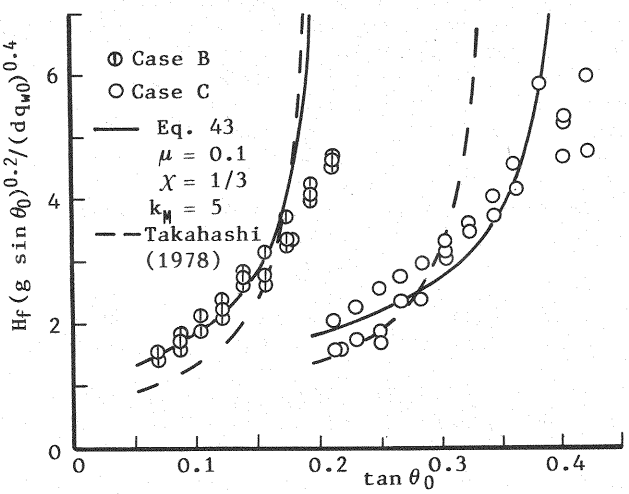

Fig. 16 Nondimensional bore height versus bed slope

$$\frac{q_t}{q_{w0}} = \frac{U_f H_f}{q_{w0}} = \frac{1}{1 - C_T/C_*} \tag{42}$$

Substituting Eq. 38 into Eq. 42, nondimensional bore height is expressed as

$$\frac{H_f(g \sin\theta_0)^{0.2}}{(d\, q_{w0})^{0.4}} = \left[\frac{C_*}{C_* - C_T}\left\{\frac{\sigma}{\rho} K_M \left(\frac{\psi}{\chi} C_*\right)^5\right\}^{1/2}\right/$$

$$\int_{C_s}^{C_*} \frac{2C - C_s}{C - C_\alpha}\left(\int_C^{C_*} F(C)dC\right)dC\Big]^{0.4} \tag{43}$$

Fig. 16 shows the theoretical curve together with the experimental results. A solid line is the result calculated by Eq. 43 and the broken line is the one deduced by Takahashi's theory. From Figs. 15 and 16, good agreement is found between the present theory and the experiments.

Lastly, it has been known that the layer of water is formed over the dense mixture of grains and water at the slope angles such that $\theta_0 < \theta_{0i}$ (8, 13). On the other hand, the authors (4) have pointed out that the layer of plug flow is formed over the shear flow at $\theta_0 > \theta_{0*}$. Therefore, this theory developed on debris flow is suitable for the angles between θ_{0i} and θ_{0*}.

CONCLUSIONS

The interparticle stresses and the characteristics of debris flow have been investigated theoretically and experimentally. The results are summarized as follows:

1. From the microscopic observations of interparticle interactions, the mechanism of grain collisions and the modes of the subsequent relative movements are made clear.
2. Most of the grains in the flow collide at the `upstream' quadrant on the surface of the relatively lower grains, and then override them until the grains separate at the `downstream' quadrant.
3. The interparticle stresses are divided into collision stress and contact stress. The former is evaluated theoretically by extending the analysis of the binary collisions to the problem of momentum transfer in many-body collisions. The latter is treated as the isotropic pressure expressed by the grain concentration. Thus, the interparticle stress components are given by Eq. 19.
4. The distributions of grain concentration and velocity in debris flow show the following features: 1) the concentration gradient becomes larger with decrease in the bed slope, 2) the velocity profile is convex upward in the lower part and inversely downward in the upper part, and thus has an inflection point in a flow. These experimental results agree well with the theoretical ones obtained by applying the above stresses to the basic equations for debris flow.
5. The characteristics of debris flow such as concentration flux, velocity and depth are predictable, as shown in Figs. 14, 15 and 16, respectively.

REFERENCES

1. Bagnold, R.A. : Experiments on a gravity-free dispersion of large solid spheres in a Newtonian fluid under shear, Proc. R. Soc. London,Ser. A, Vol.225, pp.49-63, 1954.
2. Daido, A. : Characteristics of flow containing a large number of sand grains on a steep slope, Proc. 18th Japanese Conference on Hydraulics, pp.199-203, 1974 (in Japanese).
3. Daido, A. : Constitutive equations for grain flow, 16th Symposium on Natural Disaster Science, pp.215-218, 1979(in Japanese).
4. Hashimoto, H. and T. Tsubaki : Flow properties of debris flow in a very steep channel, Proc. 27th Japanese Conference on Hydraulics, pp.285-290, 1983 (in Japanese).
5. Hirano, M. and M. Iwamoto : Experimental study on the grain sorting and the flow characteristics of a bore, Memo. of the Faculty of Engrg. Kyushu Univ., Vol.41, No.3, pp.193-202, 1981.
6. Kanatani, K : A micropolar continuum theory for the flow of granular materials, Int. J. Engng. Sci., Vol.17, pp.419-432, 1979.
7. Mctigue, D.F. : A model for stresses in shear flow of granular materials, Proc. U.S.-Japan Sem. on Continuum-Mechanical and Statistical Approaches in the Mechanics of Granular Materials, pp.266-271, 1978.
8. Mizuyama, T. : Sediment transport rate in the transition region between debris flow and bed load transport, Shin-Sabo, 116, pp.1-6, 1980.
9. Savage, S.B. and D.J. Jeffrey : The stress tensor in a granular flow at high shear rates, J. Fluid Mech., Vol.110, pp.255-272, 1981.
10. Takahashi, T. : Mechanical characteristics of debris flow, J. Hydraul. Div., ASCE, Vol.104, HY8, pp.1153-1169, 1978.
11. Takahashi, T. and H. Yoshida : Study on the deposition of debris flows (1) - Deposition due to abrupt change of bed slope, Ann. Disaster Prev. Res. Inst. Kyoto Univ., No.22B-2, pp.315-328, 1979 (in Japanese).

12. Takahashi, T. : Debris flow on prismatic open channel, J. Hydraul. Div., ASCE, Vol. 106, HY3, pp.381-396, 1980.
13. Takahashi, T. : Study on the deposition of debris flows (3) - Erosion of debris fan, Ann. Disaster Prev. Res. Inst. Kyoto Univ., No.22B-2, pp.315-328, 1979 (in Japanese).
14. Tsubaki, T., H. Hashimoto and T. Suetsugi : Grain stresses and flow properties of debris flow, Proc. Jpn. Soc. Civil Engrs. No.317, pp.79-91, 1982 (in Japanese).

APPENDIX - NOTATION

The following symbols are used in this paper:

a = numerical constant in Bagnold's formula;
C, C_* = grain concentrations in the flow and the bed;
C_b = grain concentration estimated from N_A at the bottom;
C_T, $\bar{C}$ = concentration flux and average concentration of grains;
d = grain size;
dn = number of collisions against the small surface of a grain per unit time;
$E_{j,j+1}$ = force acting on a (j+1)th-order grain from a jth-order grain;
F, $\mathbf{F}$ = normal and mean collision force;
$\mathbf{F}_z(\theta')$ = mean collision force acting on a either side of the grain surface cut by the plane S_z;
$\mathbf{F}(\theta,\phi)$ = function of θ and ϕ in Eq. 9;
h = flow depth;
H_f = height of debris bore;
I_z = vertical component of stress due to the interaction force between grains and fluid;
k_M = numerical constant related to ϵ;
K_M = coefficient in Eq. 26;
K_p = coefficient related to contact stress;
m = grain mass;
N = number density of grains;
N_A = number of grains in contact with the side wall;
n_c, n_c' = number and density of contact points on a grain;
$_jN_{j+1}$ = number of (j+1)th-order grains in contact with jth-order one
$\mathbf{n}$, $\mathbf{s}$ = unit vectors in the direction from the center of grain o to the collision point and in the sliding direction of grain i;
p = contact stress;
q_i, q_{wO} = discharges of seepage water and fresh water per unit width;
q_t = total discharge of debris flow per unit width;
S_x, S_z = planes of unit area perpendicular to the x axis and z axis;
t = time;
t_c = collision time;

T_c = mean duration of a contact between grains;

u, u_s = flow velocities at a level z and the free surface;

$\bar{u}$ = average velocity;

u_* = shear velocity;

u_i, u_i' = relative velocities of grain i to grain o before and after the collision;

U_f = moving velocity of debris bore;

x, y, z = cartesian coordinate system as defined in Fig. 1;

α = ratio of collision shear stress to the normal stress;

α_B = dynamic angle of internal friction in Bagnold's formula;

β = coefficient in Eq. 7;

γ = coefficient in Eq. 28;

δ_{ij} = Kronecker delta;

ϵ = coefficient concerning momentum transfer in many-body collisions;

$\eta = z/h$ = dimensionless form of the ordinate z;

θ, ϕ = spherical coordinates as defined in Fig. 7;

θ_0 = slope angle of bed;

θ_{0i}, θ_{0*} = critical slope angles for occurrence of debris flow and for the instability of the whole sediment bed;

κ = numerical constant in the equation of θ_{0i};

μ = coefficient of sliding friction;

ρ = fluid density;

σ = grain density;

σ_{ij} = interparticle stress component;

τ_x, τ_z = collision stress vectors on the planes S_x and S_z;

τ_{ij}, τ_{zx}, τ_{zz} = collision stress components;

Φ = angle of repose of grains in water; and

χ = numerical constant related to K_p.